European Journal of Medicinal Chemistry 104 (2015) 86–96

Contents lists available at ScienceDirect

European Journal of Medicinal Chemistry

journal homepage: http://www.elsevier.com/locate/ejmech

Research paper

Preliminary evaluation of fluoro-pegylated benzyloxybenzenes for quantification of β-amyloid plaques by positron emission tomography

Yanping Yang [a], Hualong Fu [a], Mengchao Cui [a, *], Cheng Peng [b], Zhigang Liang [b, **], Jiapei Dai [c], Zhiyong Zhang [d], Chunping Lin [d], Boli Liu [a]

[a] Key Laboratory of Radiopharmaceuticals, Ministry of Education, College of Chemistry, Beijing Normal University, Beijing 100875, PR China
[b] Department of Nuclear Medicine, Xuanwu Hospital, Capital Medical University, Beijing 100053, PR China
[c] Wuhan Institute for Neuroscience and Neuroengineering, South-Central University for Nationalities, Wuhan 430074, PR China
[d] Beijing ZHIBO Bio-Medical Technology Co. Ltd., Beijing 102502, PR China

ARTICLE INFO

Article history:
Received 25 August 2015
Received in revised form
17 September 2015
Accepted 21 September 2015
Available online 26 September 2015

Keywords:
Alzheimer's disease
β-Amyloid plaques
Benzyloxybenzenes
F-18 tracer
PET imaging

ABSTRACT

A new series of fluoro-pegylated benzyloxybenzenes were designed, synthesized and evaluated as PET probes for early detection of Aβ plaques. Molecular docking revealed that all of the flexible benzyloxybenzenes inserted themselves into the hydrophobic Val18_Phe20 cleft on the flat spine of the Aβ fiber, in a manner similar to that of IMPY molecule. The most potent probe, [^{18}F]**9a**, exhibited a combination of high binding affinity to Aβ aggregates ($K_i = 21.0 \pm 4.9$ nM), high initial brain uptake (9.14% ID/g at 2 min), fast clearance from normal brain tissue (1.79% ID/g at 60 min), and satisfactory *in vivo* biostability in the brain (95% of intact form at 2 min). [^{18}F]**9a** clearly labeled Aβ plaques in *in vitro* autoradiography of postmortem AD patients and Tg mice brain sections. *Ex vivo* autoradiography further demonstrated that [^{18}F]**9a** did penetrate the intact BBB and specifically bind to Aβ plaques *in vivo*. Overall, [^{18}F]**9a** may be a potential PET probe for imaging Aβ plaques in AD brains.

1. Introduction

In Alzheimer's disease (AD), a myriad of chemically adhesive β-amyloid (Aβ) proteins gradually stick together to form hard, insoluble plaques, which precede the characteristic behavioral and cognitive symptoms by years. Amyloid plaques are suspected to be one of the major brain abnormalities that define AD [1]. With a focus on the amyloid cascade hypothesis, a wide variety of imaging probes have been developed to sensitively measure Aβ plaques, facilitating the early diagnosis of AD and the monitoring of anti-Aβ therapeutic efficacy (Fig. 1) [2,3]. Clinical trial reports of positron emission tomography (PET) scans indicated that [^{11}C]PIB and its fluorinated alternative [^{18}F]GE-067 (flutemetamol) can be used to differentiate cognitively impaired patients from healthy controls [4,5]. Additionally, two fluoro-pegylated stilbene derivatives, [^{18}F]AV-45 (florbetapir) [6] and [^{18}F]BAY94-9172 (florbetaben) [7], can be used to visualize the amyloid load in AD brains and have received marketing authorization. However, all of the three U.S. FDA-approved ^{18}F-labeled Aβ probes exhibit a high degree of nonspecific subcortical white matter retention, which has led to uncertainty in the detection of low levels of amyloid deposits at the early stages of AD, and some findings attributed this issue to slow tracer clearance [8–10]. Therefore, further improvement of washout rates from normal brain regions could increase target-to-background ratios and quantitative accuracy of the diagnosis.

Most of the reported Aβ binding probes are variants of classic amyloid binding dyes called Congo Red (CR) and Thioflavin T, and these tracers exist in a rigid flat configuration. By breaking the extended π-conjugated systems, we have developed a novel class of radioiodinated flexible benzyloxybenzene analogs to track amyloid levels with a single-photon emission computed tomography

Abbreviations: AD, Alzheimer's disease; Aβ, β-amyloid; PET, positron emission tomography; PIB, 2-(40-(methylaminophenyl)-6-hydroxybenzothiazole; GE-067, 2-(3-fluoro-4-(methylamino)phenyl)benzo[*d*]thiazol-6-ol; AV-45, (*E*)-4-(2-(6-(2-(2-(2-fluoroethoxy)ethoxy)ethoxy)pyridin-3-yl)vinyl)-N-methylaniline; BAY94-9172, (*E*)-4-(4-(2-(2-(2-fluoroethoxy)ethoxy)ethoxy)styryl)-N-methylaniline; U.S. FDA, U.S. Food and Drug Administration; CR, Congo red; SPECT, single-photon emission computed tomography; BOB-4, 1-iodo-4-((4-methoxyphenoxy)methyl)benzene; FPEG, fluoro-pegylated; TBAF, tetra-*n*-butylammonium fluoride; THF, tetrahydrofuran; RMSD, root mean square deviations; IMPY, 2-(4'-dimethylaminophenyl)-6-iodoimidazo[1,2-*a*]pyridine; DANIR 3b, (*E*)-2-(3-(6-(dimethylamino)naphthalen-2-yl)allylidene)malononitrile.

* Corresponding author.
** Corresponding author.
E-mail addresses: cmc@bnu.edu.cn (M. Cui), zg_liang1972@sina.com (Z. Liang).

http://dx.doi.org/10.1016/j.ejmech.2015.09.028
0223-5234/

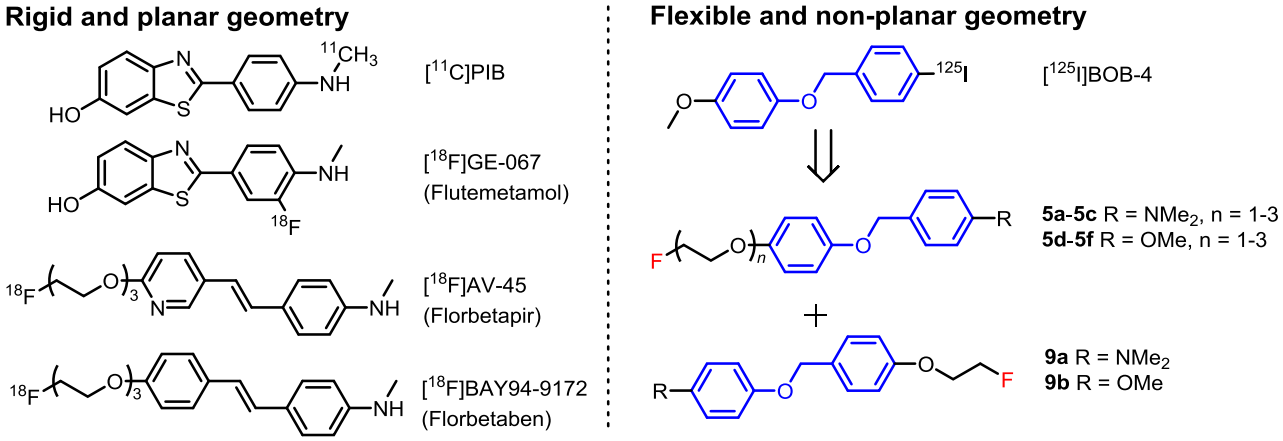

Fig. 1. Chemical structures of clinical PET tracers targeting Aβ plaques based on rigid and planar scaffolds, and the newly designed Aβ PET probes based on the flexible benzyloxybenzene scaffold.

(SPECT) scan [11]. The lead compound, [^{125}I]1-iodo-4-((4-methoxyphenoxy)methyl)benzene ([^{125}I]BOB-4), exhibited strong labeling of Aβ plaques and good kinetic profiles. This encouraging finding motivated efforts toward the exploration of ^{18}F-labeled benzyloxybenzenes for PET mapping of Aβ plaques. More recently, we reported two couples of structurally identical ^{18}F- and ^{125}I-labeled benzyloxybenzenes for PET/SPECT comparative imaging of Aβ plaques [12]. These ^{18}F-labeled ligands showed good binding potencies for Aβ aggregates and high levels of initial brain uptake; however, the slow washout rates from the normal mouse brains limited their further application for amyloid imaging *in vivo*.

During a search for PET imaging agents with improved pharmacokinetic properties, we designed a new series of fluoropegylated (FPEG) benzyloxybenzenes with a dimethylamino group or methoxy group, which are commonly used as the anchor for binding Aβ plaques. Herein, we reported the design, synthesis and biological evaluation of new FPEG benzyloxybenzenes as PET probes for quantifying Aβ plaques and tracking AD progression.

2. Results and discussion

2.1. Chemistry

Scheme 1 outlines the synthesis of the desired benzyloxybenzene derivatives and their precursors. The hydroxy group of 4-(benzyloxy)phenol was coupled with 2-chloroethanol, 2-(2-chloroethoxy)ethanol, or 2-(2-(2-chloroethoxy)ethoxy)ethanol) using an alternative base-catalyzed S_N2 reaction system (K_2CO_3/DMF) instead of KOH/EtOH reported by Xi et al. [13], providing polyethyleneglycol-modified (n = 1–3) compounds **1a**–**1c** in 60–84% yields. Tosylation of the free hydroxyl groups of **1a**–**1c** and 4-(2-hydroxyethoxy)benzaldehyde gave tosylates **2a**–**2c** and **6** in yields higher than 75%. Compounds **2a**–**2c** were successfully converted to phenols **3a**–**3c** by debenzylation with Pd/C under a hydrogen atmosphere. Compound **6** was subsequently reduced with $NaBH_4$ to afford the corresponding benzyl alcohol **7**. The Mitsunobu reaction was employed to form the benzyloxybenzene backbone from benzyl alcohols and the corresponding phenols in 57–83% yields. The fluorinated benzyloxybenzene derivatives **5a**–**5f** and **9a**–**9b** were obtained by refluxing the corresponding tosylates **4a**–**4f** and **8a**–**8b** in anhydrous TBAF/THF.

Single crystals of **5a** and **9a** were acquired by slow evaporation from ethyl acetate at room temperature. They were characterized by single-crystal X-ray diffraction, and their structures were elucidated using the SHELXL-2014 program [14]. The crystal structures of **5a** and **9a** were non-planar and the dihedral angles between the two phenyl rings were 71.5° and 68.5°, respectively (Supporting Information Fig. S1).

2.2. In vitro binding assay using Aβ aggregates

To quantitatively evaluate the binding affinities of these fluoropegylated benzyloxybenzenes to Aβ_{42} aggregates, we conducted an inhibition binding assay using [^{125}I]BOB-4 as a competitive radioligand according to conventional methods (Table 1). The FPEG benzyloxybenzenes inhibited the binding of [^{125}I]BOB-4 in a dose-dependent manner (Fig. S2 in Supplementary information). The N,N-dimethylated benzyloxybenzenes exhibited higher binding affinities than the corresponding methoxylated ligands (K_i: **5a** < **5d**, **5b** < **5e**, **5c** < **5f**, and **9a** < **9b**). This result was consistent with that of previous report [11]. As the length of FPEG increased, a decline in binding ability was observed (K_i: **5a** < **5b** < **5c**, **5d** < **5e** < **5f**), which differed from the structure-activity relationships of benzoheterocycle [15,16] and stilbene [17,18] derivatives. Among these FPEG derivatives, the N,N-dimethylated ligands **5a** and **9a** with a short FPEG side chain (n = 1) exhibited the most potent binding affinity with K_i values of 25.7 ± 2.6 and 21.0 ± 4.9 nM, respectively, which were in the same range as that of well-established IMPY (K_i = 32.2 ± 2.1 nM), PIB (K_i = 38.8 ± 2.6 nM) and AV-45 (K_i = 11.4 ± 1.1 nM) under identical assay conditions. The excellent affinities strongly suggest that **5a** and **9a** could clearly label Aβ plaques in the AD brain.

2.3. Molecular docking

To further elucidate the binding nature of these FPEG benzyloxybenzenes to Aβ fibers, computational docking studies were performed. Geometry optimizations of these FPEG benzyloxybenzenes were first performed at the B3LYP/6-31G(d, p) level in the water phase. As shown in Supporting Information Fig. S1, the optimized compounds all adopted non-planar geometries. The optimized structures of **5a** and **9a** were coincident with the geometries of their X-ray crystallographic structures, yielding root mean square deviations (RMSD) of 0.26 Å and 0.19 Å, respectively. Computational docking results indicated that all of the flexible benzyloxybenzenes rotated into near-flat geometries and bound to the hydrophobic Val18_Phe20 channel formed by side-chain ladders, resembling the behavior of IMPY molecule and other recently reported benzyloxybenzene ligands [11,12] (Fig. 2). The distribution of the calculated binding energies of the top-ranking

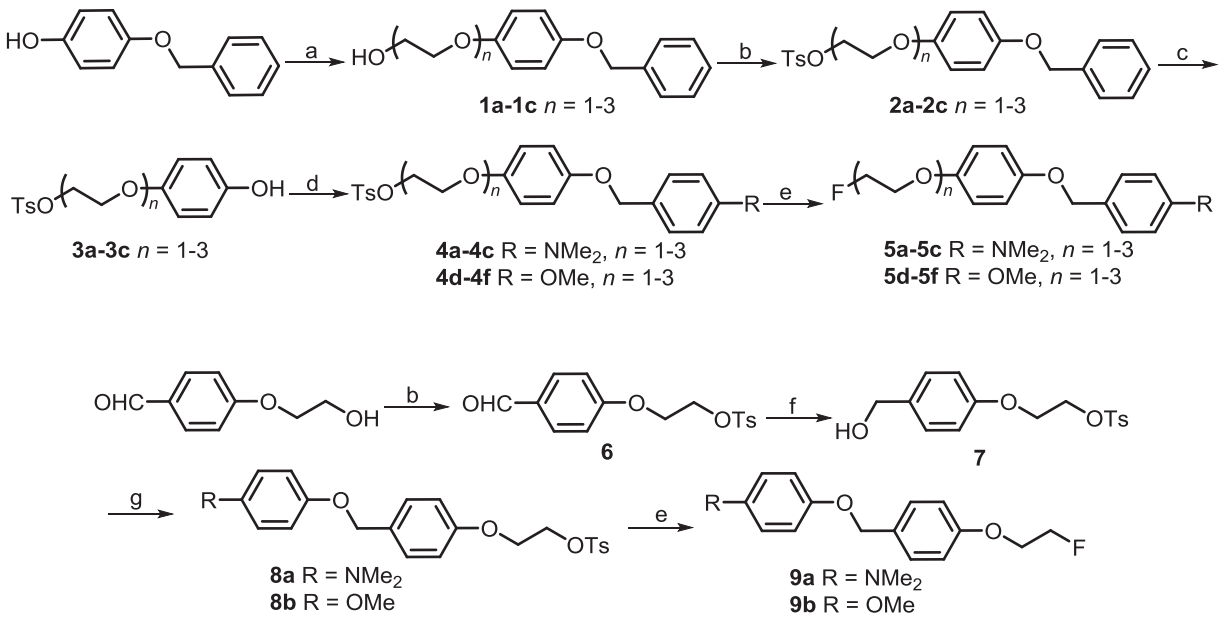

Scheme 1. Reagents and conditions: (a) 2-chloroethanol (or 2-(2-chloroethoxy)ethanol, or 2-(2-(2-chloroethoxy)ethoxy)ethanol), K_2CO_3, DMF, 90 °C; (b) TsCl, CH_2Cl_2, Et_3N, rt; (c) 10% Pd/C, 1 atm H_2, 50 °C; (d) (4-(dimethylamino)phenyl)methanol (or (4-methoxyphenyl)methanol), PPh_3, DEAD, THF, rt; (e) TBAF (1 M in THF), THF, reflux; (f) $NaBH_4$, MeOH, 0 °C; (g) 4-(dimethylamino)phenol (or 4-methoxyphenol), PPh_3, DEAD, THF, rt.

Table 1
Chemical structures and inhibition constants for the binding of [^{125}I]BOB-4 to Aβ_{42} aggregates.[a]

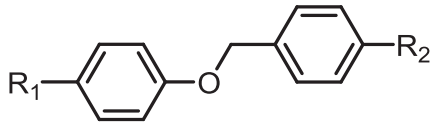

Compounds	R_1	R_2	K_i (nM)
5a	OEtF	NMe_2	25.7 ± 2.6
5b	$(OEt)_2F$	NMe_2	191.1 ± 38.4
5c	$(OEt)_3F$	NMe_2	357.7 ± 22.2
5d	OEtF	OMe	118.5 ± 34.6
5e	$(OEt)_2F$	OMe	437.9 ± 36.7
5f	$(OEt)_3F$	OMe	770.1 ± 95.0
9a	NMe_2	OEtF	21.0 ± 4.9
9b	OMe	OEtF	152.6 ± 31.6
IMPY	-	-	32.2 ± 2.1
PIB	-	-	38.8 ± 2.6
AV-45	-	-	11.4 ± 1.1

[a] Measured in triplicate with values given as the mean ± standard error.

conformations for each ligand suggested that benzyloxybenzenes with shorter FPEG side-chains fit more snugly into the binding pocket with lower binding energies, which was in agreement with the higher binding affinities. The binding energies displayed a strong qualitatively linear correlation with the experimental pK_i values with an R^2 value of 0.85 (Fig. 2e).

2.4. Radiochemistry

The most promising ligands **5a** and **9a**, along with three methoxylated ligands **5d**, **5f** and **9b**, were selected for ^{18}F radiolabeling. The radiofluorination was performed on the corresponding tosylate precursors through a nucleophilic substitution with the [^{18}F]fluoride anion (Scheme 2), reproducibly giving the radiofluorinated ligands in radiochemical yields of 26–32% with a specific activity of approximately 130 GBq/μmol at the end of synthesis. The radiochemical purity was greater than 98% after HPLC purification. The identities of these radiotracers were verified by a comparison of retention times with the corresponding nonradioactive compounds in co-injection HPLC analysis (Table S2, Fig. S3 in Supplementary information).

2.5. In vitro autoradiography

To further characterize the binding affinities to Aβ plaques, *in vitro* autoradiography was performed on brain sections from AD patients and Tg model mice. As observed in Fig. 3a, b, d, e and Fig. 4a, c, autoradiographic images of [^{18}F]**5a** and [^{18}F]**9a** (K_i = 25.7 and 21.0 nM, respectively) showed clusters of hot spots on the cerebral cortex sections of the AD patients (n = 2) and Tg mouse brains, which was highly consistent with the fluorescent specks stained with DANIR 3b, a fluorescent probe targeting Aβ plaques [19]. Moreover, low radioactivity accumulation was observed in white matter. Conversely, no binding signals on healthy human and wild-type mouse brain sections were observed (Fig. 3c, f and Fig. 4b, d). This result suggested that [^{18}F]**5a** and [^{18}F]**9a** are promising tracers to image Aβ plaques with low non-specific binding and high signal sensitivity. [^{18}F]**5d** and [^{18}F]**9b** with a K_i of 118.5 and 152.6 nM, respectively, exhibited moderate binding to Aβ plaques, and [^{18}F]**5f** with a K_i of 770.1 nM exhibited weak binding and labeled only a few Aβ plaques (Fig. S4 in Supplementary information). The results of the *in vitro* autoradiography were consistent with those of the *in vitro* binding assay, and also suggested that the substituent (N,N-dimethyl or methoxyl) and FPEG length could affect the binding affinities of benzyloxybenzene derivatives for Aβ plaques.

2.6. In vivo biodistribution

To evaluate the brain uptake and washout properties of these ^{18}F-labeled benzyloxybenzenes, partition coefficient determination and biodistribution of radioactivity in normal ICR mice were performed. The log D values ranged between 2.75 and 3.65, indicating

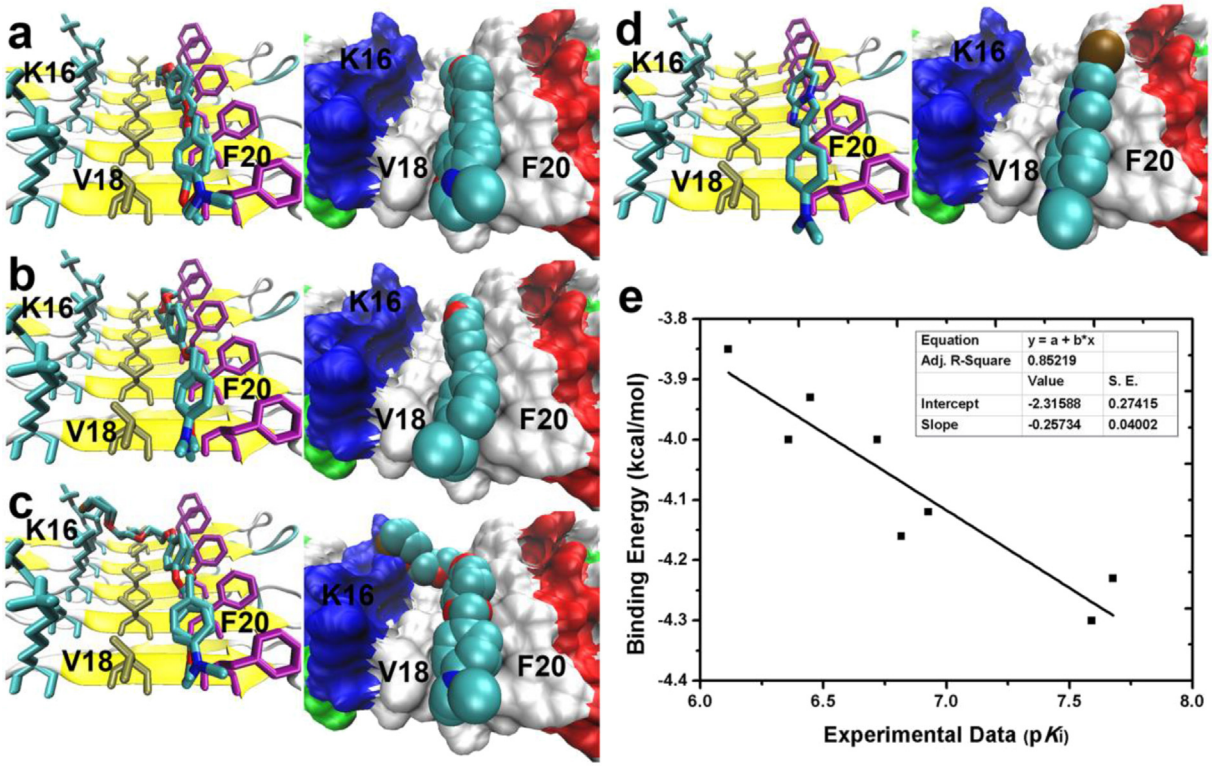

Fig. 2. Molecular docking results of the FPEG benzyloxybenzenes on Aβ fibers (PDB ID: 2LMO). Lowest energy docked conformations of $n = 1$ FPEG compounds **5a**, **5d**, **9a** and **9b** (a); $n = 2$ FPEG compounds **5b** and **5e** (b); $n = 3$ FPEG compounds **5c** and **5f** (c); and IMPY (d) inserted into the hydrophobic Val18_Phe20 cavity on the flat β-sheet surface. (e) The calculated binding energies showed a linear correlation with experimental pK_i values in high R^2 value of 0.85.

that these ^{18}F-labeled benzyloxybenzenes have lipophilicity values that are suitable for passage through the blood brain barrier (BBB) (Supporting Information Table S3). The ^{18}F-labeled tracers penetrated the BBB with initial brain uptake levels of 4.51–9.95% ID/g at 2 min post-injection and dropped to 0.71–2.33% ID/g at 60 min post-injection (Fig. 5). Most of all, [^{18}F]**9a** combined a high binding affinity to Aβ plaques ($K_i = 21.0 \pm 4.9$ nM), high initial brain uptake (9.14% ID/g at 2 min) and rapid clearance with a brain$_{2\ min}$/brain$_{60\ min}$ ratio of 5.1. Compared with reported biodistribution data for [^{18}F]AV-45 [20], which displayed moderate brain uptake (7.33% ID/g at 2 min) and clearance rate with a brain$_{2\ min}$/brain$_{60\ min}$ ratio of 3.9, [^{18}F]**9a** gained an advantage over [^{18}F]AV-45. Because there are no Aβ plaques in the brain of normal mice, [^{18}F]**9a** with higher washout index is preferred. Methoxylated $n = 1$ FPEG ligands [^{18}F]**5d** and [^{18}F]**9b** exhibited slow accumulation of radioactivity in bone with the time post-injection. In contrast, no marked bone uptake of radioactivity was observed for [^{18}F]**5a**, [^{18}F]**9a** and [^{18}F]**5f** (1.52–2.38% ID/g at 60 min post-injection), indicating little defluorination *in vivo*.

2.7. In vivo metabolism in mice

The brain washouts of the left-substituted FPEG ligands ([^{18}F]**5a** and [^{18}F]**5d**) were faster in comparison to the right-substituted FPEG ligands ([^{18}F]**9a** and [^{18}F]**9b**). To address this observation, the *in vivo* metabolism of a pair of N,N-dimethylated benzyloxybenzenes ([^{18}F]**5a** and [^{18}F]**9a**) in normal ICR mice was characterized at different post-injection time points. The recovery of radioactivity was calculated to be approximately 70% (decay-corrected). HPLC analysis of selected organ samples provided the percent ratio of the radioactive parent tracers and metabolites to total radioactivity (no decay correction). Fig. 6 showed the

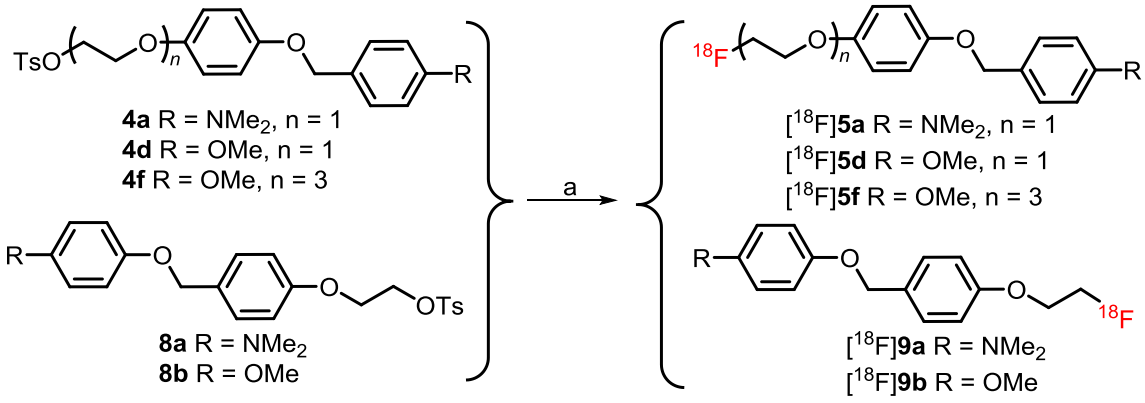

Scheme 2. Reagents and conditions: Kryptofix 222/K_2CO_3, $^{18}F^-$, MeCN, 100 °C, 5 min.

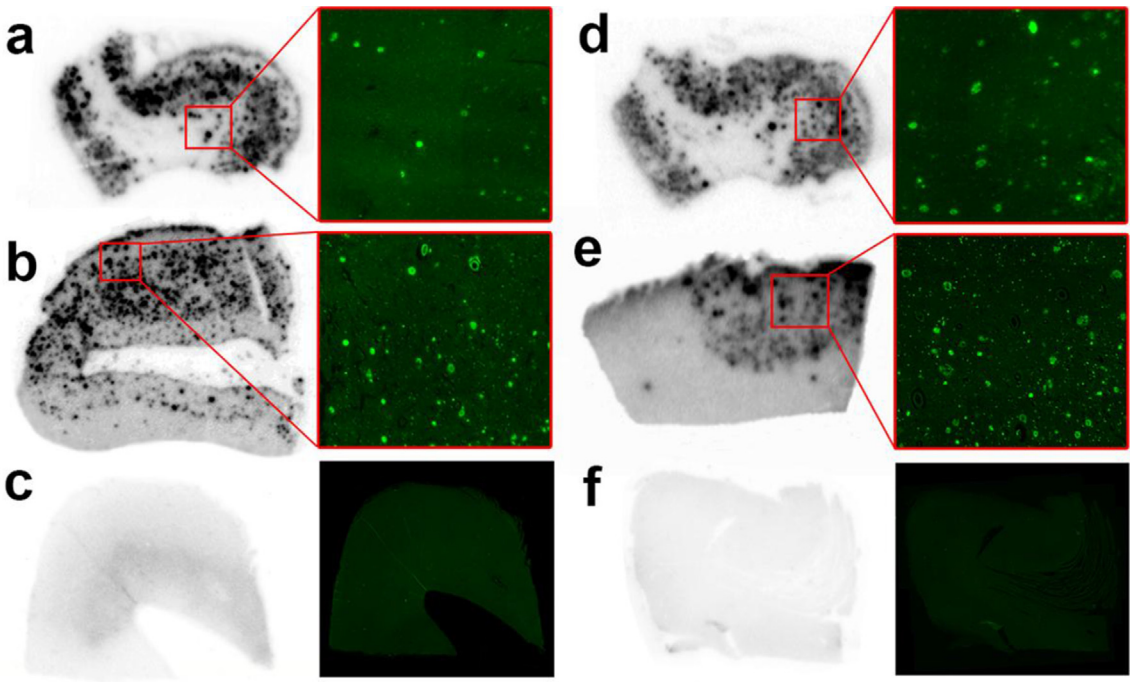

Fig. 3. *In vitro* autoradiography of [^{18}F]**5a** (a–c) and [^{18}F]**9a** (d–f) on human brain sections. (a and d) AD case 1: male, 91 years old; (b and e) AD case 2: female, 64 years old; (c and f) Healthy case: female, 89 years old. Fluorescence staining using DANIR 3b presented on the right panel of each image confirmed the location and distribution of plaques.

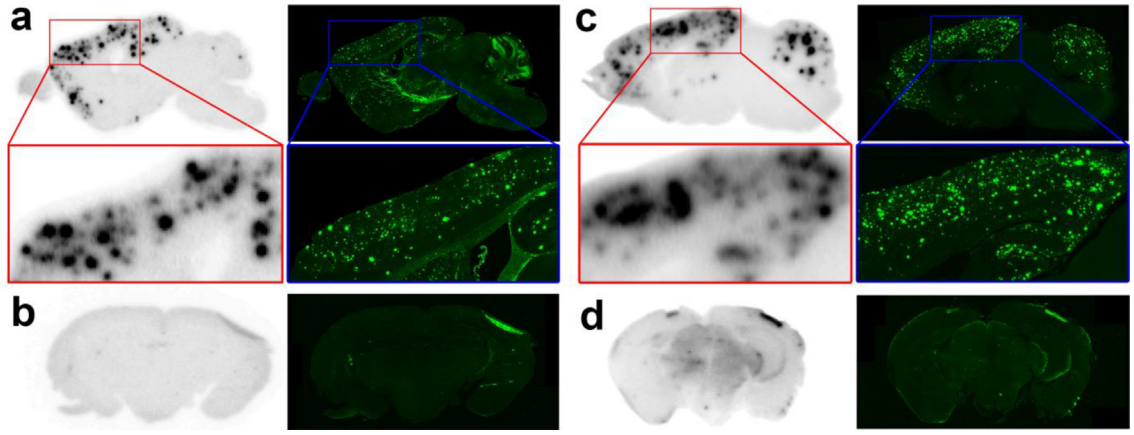

Fig. 4. *In vitro* autoradiography of [^{18}F]**5a** (a–b) and [^{18}F]**9a** (c–d) on mice brain sections. (a and c) Tg mouse brain sections, C57BL6, APPswe/PSEN1, 11 months old; (b and d) wild-type mouse brain sections, C57BL6, 11 months old. The presence and location of plaques were confirmed with fluorescence staining using DANIR 3b.

percentages of the intact [^{18}F]ligands in the brain, plasma and liver of mice, while detailed metabolism data were shown in Table S4 and Table S5 in the Supplementary information section. [^{18}F]**5a** and [^{18}F]**9a** each degraded into six corresponding polar radioactive metabolites with shorter retention times. [^{18}F]**5a** and [^{18}F]**9a** exhibited good biostability in the brain with 76.7% and 95.4% of the parent tracers presented at 2 min, respectively. At 30 min, 20.6% and 31.6% of unchanged [^{18}F]**5a** and [^{18}F]**9a** remained in the brain. In plasma, fractions corresponding to intact [^{18}F]**9a** decreased to 56.5% at 2 min, and steadily dropped to 5.8% at 30 min. However, [^{18}F]**5a** was more extensively converted to polar metabolites, leaving only approximately 10% of intact [^{18}F]**5a** in plasma at 2 min. After 30 min, no parent [^{18}F]**5a** was detected in plasma, and all of the radioactivity was found to be polar metabolites ([^{18}F]**M5a-1** and [^{18}F]**M5a-2**). In liver, unmetabolized [^{18}F]**9a** constituted 63.5% of the total radioactivity at 2 min. In contrast, the breakdown of [^{18}F]**5a** was so remarkable that only approximately 20% of the radioactivity was presented in its intact form at 2 min, consistent with the results in plasma. As estimated from HPLC retention times, the major metabolites [^{18}F]**M5a-1** (t_R = 2.8 min) and [^{18}F]**M5a-2** (t_R = 3.4 min) in plasma and liver were much more polar than the intact [^{18}F]**5a** (t_R = 9.1 min). The polar and hydrophilic metabolites generated in liver can enter the bloodstream, spread through the circulation of blood, and then be absorbed by the intestine and excreted from the body with urine. The faster metabolism of [^{18}F]**5a** in liver may be the reason for its faster clearance from the normal brain relative to [^{18}F]**9a**. In the urine samples, the amount of radioactivity was low at the early stages and then increased dramatically with time. No parent tracers were observed in urine and the polar metabolites [^{18}F]**M5a-1** (t_R = 2.8 min) and [^{18}F]**M9a-1** (t_R = 2.7 min) account for 100% and 70% of the total radioactivity. This result indicated that the polar metabolites were cleared

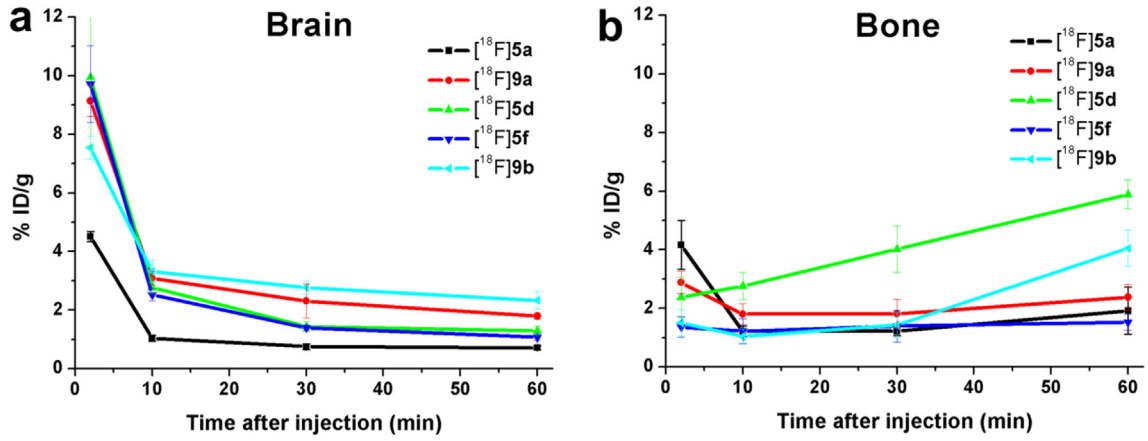

Fig. 5. Line charts of brain and bone uptakes of five ^{18}F-labeled benzyloxybenzenes in normal ICR mice (n = 5–6).

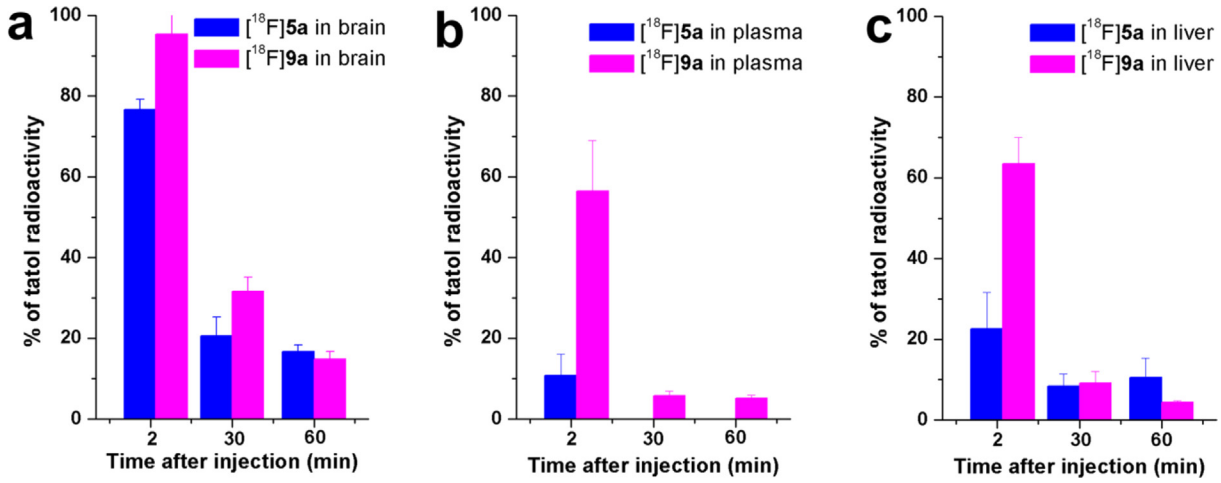

Fig. 6. Percentages of parent tracers extracted from the brain (a), plasma (b) and liver (c) of ICR mice after intravenous injection of [^{18}F]**5a** and [^{18}F]**9a** (35–45 MBq) (n = 2–3).

predominantly through urine.

2.8. Ex vivo autoradiography

To confirm the specific binding of [^{18}F]**9a** to Aβ plaques *in vivo*, *ex vivo* autoradiographic studies were conducted on a Tg mouse (C57BL6, APPswe/PSEN1, male, 15 months old) and an age-matched wild-type mouse (C57BL6, male, 15 months old). Twenty minutes after injection of 1 mCi of [^{18}F]**9a** through the tail vein, the brains were removed, quickly frozen and sectioned for *ex vivo* autoradiography. Autoradiographic images showed a distinct labeling of Aβ plaques in the cortex, hippocampus and cerebellum regions of Tg mouse brain slices, whereas no such labeling was observed in the wild-type mouse brain (Fig. 7). The locations and distributions of Aβ plaques were confirmed by costaining the same brain sections with DANIR 3b. These results demonstrated that [^{18}F]**9a** did penetrate the intact BBB and bind to Aβ plaques specifically *in vivo*.

3. Conclusion

Aβ plaques are a pathological hallmark of AD, a progressive and often fatal disease, and are therefore important targets for developing PET imaging agents of AD. In this study, we synthesized and evaluated a new series of FPEG benzyloxybenzenes to quantify Aβ plaques and achieve early diagnosis of AD. The N,N-dimethylated n = 1 FPEG ligands **5a** (K_i = 25.7 nM) and **9a** (K_i = 21.0 nM) exhibited high binding affinities to Aβ aggregates, which was comparable to IMPY, PIB and AV-45 under the same conditions. Molecular docking results determined that all of the flexible FPEG benzyloxybenzenes inserted into the hydrophobic Val18_Phe20 binding pocket on the flat spine of Aβ fiber, and the molecules were locked into near-flat geometries. The calculated binding energies showed a good qualitatively linear correlation with the experimental pK_i values. *In vitro* autoradiography further confirmed the high binding affinities of [^{18}F]**5a** and [^{18}F]**9a**. Both of them showed clear labeling of Aβ plaques in the brain sections of AD patients and Tg mouse. In biodistribution, the most potent [^{18}F]**9a** exhibited high initial brain uptake level (9.14% ID/g at 2 min) and fast washout ($brain_{2\ min}/brain_{60\ min}$ ratio = 5.1). In metabolism studies, left-substituted FPEG [^{18}F]**5a** exhibited a greater degree of degradation than right-substituted FPEG [^{18}F]**9a** in plasma and liver, and the polar metabolic products can be absorbed by the intestine and excreted from the body with the urine. These data explained the faster brain clearance of left-substituted FPEG [^{18}F]**5a**. In addition, [^{18}F]**5a** and [^{18}F]**9a** showed good biostability in brain with 76.7% and 95.4% of parent tracers presented at 2 min, respectively. *Ex vivo* autoradiography of [^{18}F]**9a** confirmed its BBB penetrability and *in vivo* binding abilities to Aβ plaques. In summary, the most potent [^{18}F]**9a** satisfies most of the prerequisites for a successful Aβ PET imaging agent both *in vitro* and *in vivo*.

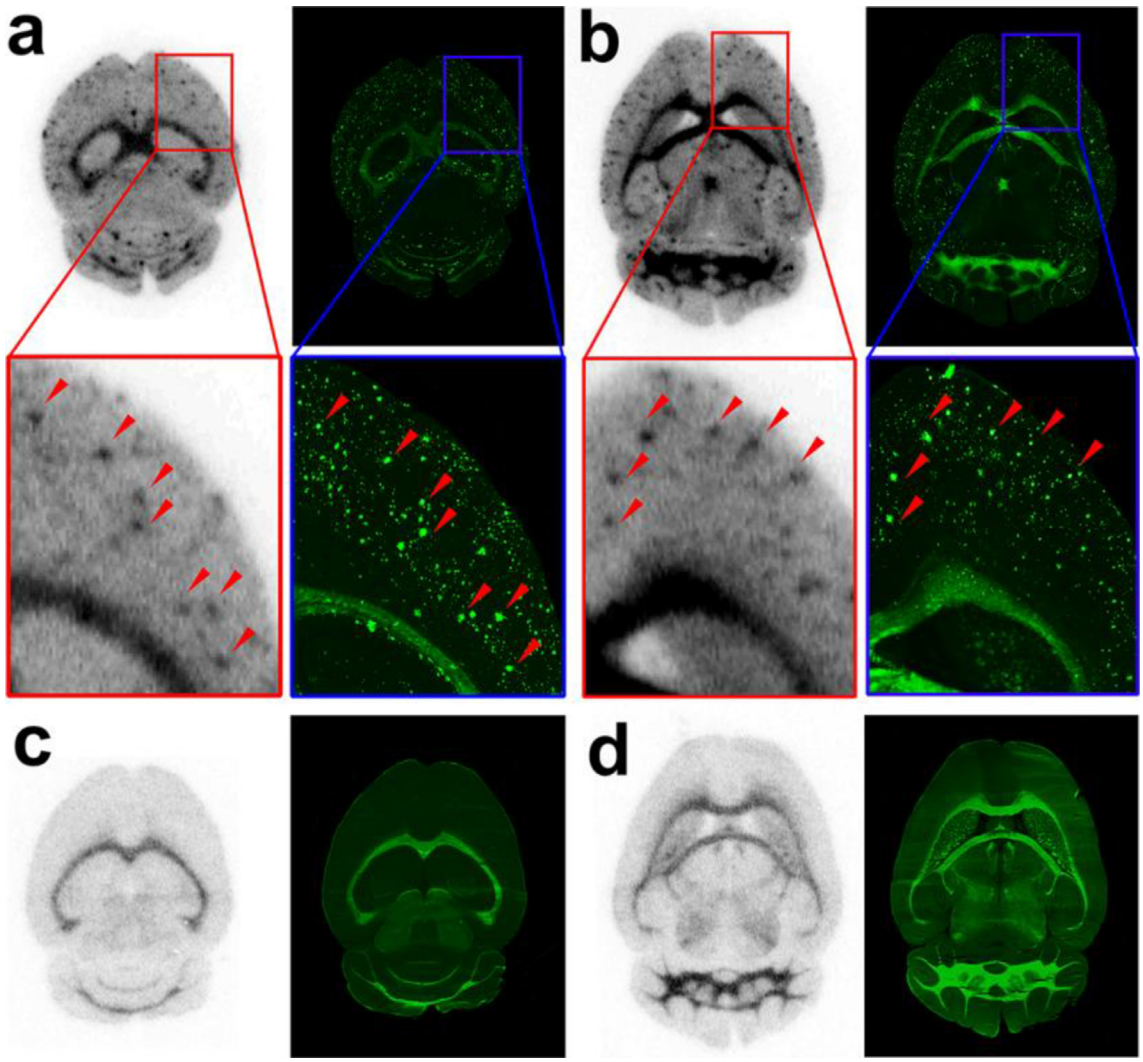

Fig. 7. *Ex vivo* autoradiography of [^{18}F]**9a**. (a–b) Different coronal brain sections of a Tg mouse (C57BL6, APPswe/PSEN1, male, 15 months old). (c–d) Corresponding coronal brain sections of an age-matched wild-type mouse (C57BL6, male, 15 months old). The Aβ plaques were confirmed by *in vitro* costaining the same brain sections with DANIR 3b.

4. Methods

4.1. General remarks

A structural model of Aβ fibers (PDB ID: 2LMO [21]) derived from solid state NMR was downloaded from the RCSB Protein Data Bank (www.rcsb.org/pdb). Geometric optimization was performed using Gaussian 09 [22] at the B3LYP/6-31G(d, p) level in the water phase. Molecular docking was performed using AutoDock4.0 [23], and the docking results were graphed using VMD 1.9.1 software [24]. All reagents for chemical synthesis were commercial products and used without further purification. $^{18}F^{-}$ was kindly provided by the Xuanwu Hospital. ^{1}H and ^{13}C NMR spectra were recorded on a Bruker Avance III NMR spectrometer (400 MHz for ^{1}H; 100 MHz for ^{13}C) in $CDCl_3$ or DMSO-d_6 solutions at room temperature. Mass spectra were acquired with a GCT CA127 Micronass UK instrument and a solariX mass spectrometer. X-ray crystallographic data for compounds **5a** and **9a** were collected on a Bruker Smart APEX II diffractometer (Bruker Co., Germany) and deposited at the Cambridge Crystallographic Data Centre as a supplementary publication (no. CCDC 1407327 for **5a**; 1407325 for **9a**). HPLC analysis was performed on a Shimadzu SCL-20 AVP equipped with a Bioscan Flow Count 3200 NaI/PMT γ-radiation scintillation detector and a SPD-20A UV detector, $\lambda = 254$ nm. A Venusil MP C18 reverse phase column (Agela Technologies, 5 μm, 10 $\times$ 250 mm) was used for separations and purity determinations with a binary gradient system (acetonitrile: water = 70%: 30%) at a 4.0 mL/min flow rate. HPLC analysis of metabolic samples was conducted on a Waters 5C18-AR-II reverse-phase column (5 μm, 10 $\times$ 250 mm). Fluorescent observation was performed on the Axio Observer Z1 inverted fluorescence microscope (Zeiss, Germany) equipped with a AF488 filter set. Post-mortem brain sections from two autopsy-confirmed AD subjects (64 years old, female; 91 years old, male, temporal lobe) and a control subject (89 years old, female, temporal lobe) were acquired from the Chinese Brain Bank Center. Transgenic mice (C57BL6, APPswe/PSEN1, male) and wild-type mice (C57BL6, male) were purchased from the Institute of Laboratory Animal Science, Chinese Academy of Medical Sciences. Normal ICR mice (20–22 g, male) used for *in vivo* biodistribution were purchased from Beijing Vital River Laboratory Animal Technology Co, Ltd. All experiments on mice were performed in accordance with the guidelines approved by the animal care committee of Beijing Normal University.

4.2. 2-(4-(benzyloxy)phenoxy)ethanol (*1a*)

In contrast to the procedure reported by Xi et al. [13], K_2CO_3 and DMF were used to prepare **1a** instead of KOH and EtOH. To a

mixture of 4-(benzyloxy)phenol (4.00 g, 20.0 mmol) and K_2CO_3 (4.15 g, 30.0 mmol) in anhydrous DMF (20 mL) was added 2-chloroethanol (2.01 g, 25.0 mmol) dropwise. The mixture was stirred at 90 °C for 4 h, and the solvent was removed by vacuum. A white precipitate was formed by adding 50 mL of 1 M NaOH, which was collected by filtration, washed with 50 mL of water and recrystallized from methanol to give **1a** as a white solid (3.46 g, 71%). m.p. 105.8–106.4 °C. ^{1}H NMR (400 MHz, $CDCl_3$) δ 7.46–7.30 (m, 5H, Ph), 6.91 (d, J = 9.1 Hz, 2H, Ph), 6.85 (d, J = 9.0 Hz, 2H, Ph), 5.02 (s, 2H, OCH_2), 4.08–3.99 (m, 2H, CH_2), 3.97–3.87 (m, 2H, CH_2), 1.95 (s, 1H, OH). MS (EI): *m/z* calcd for $C_{15}H_{16}O_3$ 244; found 244 $[M]^+$.

4.3. 2-(2-(4-(benzyloxy)phenoxy)ethoxy)ethanol (**1b**)

Instead of using 2-(2-hydroxyethoxy)ethyl 4-methylbenzenesulfonate as reactant [25], 2-(2-chloroethoxy) ethanol was applied to prepare **1b** through the same procedure as described above to prepare **1a**, giving **1b** as a white solid (894.7 mg, 84%). m.p. 75.1–75.5 °C. ^{1}H NMR (400 MHz, $CDCl_3$) δ 7.44–7.29 (m, 5H, Ph), 6.90 (d, J = 9.3 Hz, 2H, Ph), 6.85 (d, J = 9.3 Hz, 2H, Ph), 5.01 (s, 2H, OCH_2), 4.11–4.07 (m, 2H, CH_2), 3.86–3.83 (m, 2H, CH_2), 3.78–3.74 (m, 2H, CH_2), 3.69–3.65 (m, 2H, CH_2), 2.16 (s, 1H, OH). MS (EI): *m/z* calcd for $C_{17}H_{20}O_4$ 288; found 288 $[M]^+$.

4.4. 2-(2-(2-(4-(benzyloxy)phenoxy)ethoxy)ethoxy)ethanol (**1c**)

Instead of using 2-(2-(2-hydroxyethoxy)ethoxy)ethyl 4-methylbenzenesulfonate as substrate [25], 2-(2-(2-chloroethoxy) ethoxy)ethanol was applied to prepare **1c** through the same procedure as described above to prepare **1a**, giving **1c** as a white solid (4.02 g, 60%). m.p. 41.6–42.1 °C. ^{1}H NMR (400 MHz, $CDCl_3$) δ 7.46–7.29 (m, 5H, Ph), 6.93–6.81 (m, 4H, Ph), 5.01 (s, 2H, OCH_2), 4.12–4.02 (m, 2H, CH_2), 3.86–3.79 (m, 2H, CH_2), 3.75–3.67 (m, 6H, CH_2), 3.64–3.59 (m, 2H, CH_2), 2.16 (s, 1H, OH). MS (EI): *m/z* calcd for $C_{19}H_{24}O_5$ 332; found 332 $[M]^+$.

4.5. 2-(4-(benzyloxy)phenoxy)ethyl 4-methylbenzenesulfonate (**2a**)

A solution of **1a** (785.1 mg, 3.21 mmol) and Et_3N (5 mL) in anhydrous CH_2Cl_2 (10 mL) was stirred in an ice bath, and tosyl chloride (919.0 mg, 4.82 mmol) was slowly added. The reaction mixture was stirred for 4 h at room temperature and evaporated under reduced pressure. Water was added (50 mL), and the mixture was extracted by CH_2Cl_2 (3 × 10 mL). Combined organic layers were dried over anhydrous $MgSO_4$, filtered and concentrated in vacuo. Silica gel chromatography purification (petroleum ether/AcOEt = 4/1, v/v) gave **2a** as a white solid (966.2 mg, 76%). m.p. 83.1–83.7 °C. ^{1}H NMR (400 MHz, $CDCl_3$) δ 7.81 (d, J = 8.3 Hz, 2H, Ph), 7.43–7.30 (m, 7H, Ph), 6.86 (d, J = 9.1 Hz, 2H, Ph), 6.72 (d, J = 9.1 Hz, 2H, Ph), 5.00 (s, 2H, OCH_2), 4.35–4.32 (m, 2H, CH_2), 4.11–4.07 (m, 2H, CH_2), 2.44 (s, 3H, CH_3). MS (EI): *m/z* calcd for $C_{22}H_{22}O_5S$ 398; found 398 $[M]^+$.

4.6. 2-(2-(4-(benzyloxy)phenoxy)ethoxy)ethyl 4-methylbenzenesulfonate (**2b**)

The reaction described above to prepare **2a** was employed to give **2b** as a white solid from **1b** (699.2 mg, 85%). m.p. 71.5–72.1 °C. ^{1}H NMR (400 MHz, $CDCl_3$) δ 7.79 (d, J = 8.3 Hz, 2H, Ph), 7.44–7.27 (m, 7H, Ph), 6.89 (d, J = 9.2 Hz, 2H, Ph), 6.81 (d, J = 9.2 Hz, 2H, Ph), 5.02 (s, 2H, OCH_2), 4.21–4.17 (m, 2H, CH_2), 4.01–3.97 (m, 2H, CH_2), 3.77–3.73 (m, 4H, CH_2), 2.41 (s, 3H, CH_3). MS (EI): *m/z* calcd for $C_{24}H_{26}O_6S$ 442; found 442 $[M]^+$.

4.7. 2-(2-(2-(4-(benzyloxy)phenoxy)ethoxy)ethoxy)ethyl 4-methylbenzenesulfonate (**2c**)

The reaction described above to prepare **2a** was employed to give **2c** as a colorless oil from **1c** (6.37 g, 85%). ^{1}H NMR (400 MHz, $CDCl_3$) δ 7.79 (d, J = 8.3 Hz, 2H, Ph), 7.44–7.29 (m, 7H, Ph), 6.89 (d, J = 9.3 Hz, 2H, Ph), 6.84 (d, J = 9.3 Hz, 2H, Ph), 5.01 (s, 2H, OCH_2), 4.18–4.14 (m, 2H, CH_2), 4.07–4.03 (m, 2H, CH_2), 3.81–3.77 (m, 2H, CH_2), 3.71–3.67 (m, 2H, CH_2), 3.66–3.63 (m, 2H, CH_2), 3.62–3.59 (m, 2H, CH_2), 2.42 (s, 3H, CH_3). MS (EI): *m/z* calcd for $C_{26}H_{30}O_7S$ 486; found 486 $[M]^+$.

4.8. 2-(4-hydroxyphenoxy)ethyl 4-methylbenzenesulfonate (**3a**)

To a solution of **2a** (518.2 g, 1.30 mmol) in anhydrous MeOH (10 mL) was added 10% Pd/C (13.8 mg, 0.13 mmol). The mixture was stirred for 4 h at 50 °C under 1 atm of hydrogen atmosphere. The catalyst was filtered while hot and washed with MeOH, and the filtrate was concentrated in vacuo to give **3a** as a colorless oil (378.8 mg, 95%). ^{1}H NMR (400 MHz, $CDCl_3$) δ 7.82 (d, J = 8.3 Hz, 2H, Ph), 7.34 (d, J = 8.2 Hz, 2H, Ph), 6.73 (d, J = 9.1 Hz, 2H, Ph), 6.67 (d, J = 9.1 Hz, 2H, Ph), 4.35–4.31 (m, 2H, CH_2), 4.11–4.06 (m, 2H, CH_2), 3.41 (s, 1H, OH), 2.45 (s, 3H, CH_3). MS (EI): *m/z* calcd for $C_{15}H_{16}O_5S$ 308; found 308 $[M]^+$.

4.9. 2-(2-(4-hydroxyphenoxy)ethoxy)ethyl 4-methylbenzenesulfonate (**3b**)

The reaction described above to prepare **3a** was employed to give **3b** as a colorless oil from **2b** (427.0 mg, 99%). ^{1}H NMR (400 MHz, $CDCl_3$) δ 7.79 (d, J = 8.3 Hz, 2H, Ph), 7.30 (d, J = 8.0 Hz, 2H, Ph), 6.79–6.72 (m, 4H, Ph), 4.77 (s, 1H, OH), 4.21–4.17 (m, 2H, CH_2), 4.00–3.96 (m, 2H, CH_2), 3.77–3.73 (m, 4H, CH_2), 2.41 (s, 3H, CH_3). MS (EI): *m/z* calcd for $C_{17}H_{20}O_6S$ 352; found 352 $[M]^+$.

4.10. 2-(2-(2-(4-hydroxyphenoxy)ethoxy)ethoxy)ethyl 4-methylbenzenesulfonate (**3c**)

The reaction described above to prepare **3a** was employed to give **3c** as a colorless oil from **2c** (1.89 g, 91%). ^{1}H NMR (400 MHz, $CDCl_3$) δ 7.79 (d, J = 8.3 Hz, 2H, Ph), 7.32 (d, J = 8.0 Hz, 2H, Ph), 6.79–6.72 (m, 4H, Ph), 4.17–4.14 (m, 2H, CH_2), 4.05–4.02 (m, 2H, CH_2), 3.80–3.77 (m, 2H, CH_2), 3.70–3.67 (m, 2H, CH_2), 3.67–3.64 (m, 2H, CH_2), 3.63–3.59 (m, 2H, CH_2), 2.43 (s, 3H, CH_3). MS (EI): *m/z* calcd for $C_{19}H_{24}O_7S$ 396; found 396 $[M]^+$.

4.11. 2-(4-((4-(dimethylamino)benzyl)oxy)phenoxy)ethyl 4-methylbenzenesulfonate (**4a**)

A mixture of **3a** (235.4 mg, 0.76 mmol), (4-(dimethylamino) phenyl)methanol (151.4 mg, 0.76 mmol) and triphenylphosphine (300.2 mg, 1.14 mmol) in anhydrous THF (20 mL) was added dropwise with a solution of diethyl azodicarboxyate (198.5 mg, 1.14 mmol) in THF (5 mL). The mixture was stirred at room temperature under N_2 atmosphere for 4 h. Evaporation, silica gel chromatography purification (petroleum ether/AcOEt = 4/1, v/v) and recrystallization from ethyl acetate afforded **4a** as a white solid (218.6 mg, 65%). m.p. 152.3–152.7 °C. ^{1}H NMR (400 MHz, $CDCl_3$) δ 7.81 (d, J = 8.3 Hz, 2H, Ph), 7.33 (d, J = 8.0 Hz, 2H, Ph), 7.28 (d, J = 8.8 Hz, 2H, Ph), 6.85 (d, J = 9.1 Hz, 2H, Ph), 6.75–6.68 (m, 4H, Ph), 4.88 (s, 2H, OCH_2), 4.35–4.31 (m, 2H, CH_2), 4.11–4.07 (m, 2H, CH_2), 2.95 (s, 6H, $N(CH_3)_2$), 2.44 (s, 3H, CH_3); ^{13}C NMR (101 MHz, $CDCl_3$) δ 153.79, 152.13, 150.53, 144.87, 133.00, 129.83, 129.18, 127.99, 124.62, 115.86, 115.72, 112.49, 70.82, 68.28, 66.24, 40.56, 21.62. MS (ESI): *m/z* calcd for $C_{24}H_{28}NO_5S$ 442.2; found 442.3

$[M+H]^+$.

4.12. 2-(2-(4-((4-(dimethylamino)benzyl)oxy)phenoxy)ethoxy) ethyl 4-methylbenzenesulfonate (**4b**)

The reaction described above to prepare **4a** was employed to give **4b** as a white solid from **3b** (394.7 mg, 69%). m.p. 101.1–101.6 °C. ^{1}H NMR (400 MHz, $CDCl_3$) δ 7.79 (d, J = 8.3 Hz, 2H, Ph), 7.31–7.27 (m, 4H, Ph), 6.89 (d, J = 9.2 Hz, 2H, Ph), 6.80 (d, J = 9.2 Hz, 2H, Ph), 6.73 (d, J = 8.7 Hz, 2H, Ph), 4.89 (s, 2H, OCH_2), 4.21–4.17 (m, 2H, CH_2), 4.00–3.96 (m, 2H, CH_2), 3.77–3.73 (m, 4H, CH_2), 2.95 (s, 6H, $N(CH_3)_2$), 2.41 (s, 3H, CH_3); ^{13}C NMR (101 MHz, $CDCl_3$) δ 153.50, 152.80, 150.50, 144.77, 133.03, 129.80, 129.18, 127.96, 124.75, 115.88, 115.56, 112.51, 70.85, 69.98, 69.26, 68.83, 68.06, 40.57, 21.59. MS (ESI): *m/z* calcd for $C_{26}H_{32}NO_6S$ 486.2; found 486.2 $[M+H]^+$.

4.13. 2-(2-(2-(4-((4-(dimethylamino)benzyl)oxy)phenoxy)ethoxy) ethoxy)ethyl 4-methylbenzenesulfonate (**4c**)

The reaction described above to prepare **4a** was employed to give **4c** as a white solid from **3c** (986.3 mg, 70%). m.p. 72.2–72.8 °C. ^{1}H NMR (400 MHz, $CDCl_3$) δ 7.79 (d, J = 8.3 Hz, 2H, Ph), 7.32 (d, J = 8.0 Hz, 2H, Ph), 7.29 (d, J = 8.3 Hz, 2H, Ph), 6.89 (d, J = 9.2 Hz, 2H, Ph), 6.83 (d, J = 9.2 Hz, 2H, Ph), 6.79–6.69 (m, 2H, Ph), 4.89 (s, 2H, OCH_2), 4.18–4.14 (m, 2H, CH_2), 4.08–4.03 (m, 2H, CH_2), 3.81–3.76 (m, 2H, CH_2), 3.71–3.67 (m, 2H, CH_2), 3.66–3.63 (m, 2H, CH_2), 3.62–3.58 (m, 2H, CH_2), 2.96 (s, 6H, $N(CH_3)_2$), 2.43 (s, 3H, CH_3); ^{13}C NMR (101 MHz, $CDCl_3$) δ 153.45, 152.93, 150.48, 144.77, 133.09, 129.81, 129.20, 127.97, 124.88, 115.87, 115.60, 112.58, 70.86, 70.80, 70.74, 69.93, 69.25, 68.73, 68.10, 40.63, 21.61. MS (ESI): *m/z* calcd for $C_{28}H_{36}NO_7S$ 530.2; found 530.1 $[M+H]^+$.

4.14. 2-(4-((4-methoxybenzyl)oxy)phenoxy)ethyl 4-methylbenzenesulfonate (**4d**)

The reaction described above to prepare **4a** was employed to give **4d** as a white solid from **3a** and (4-methoxyphenyl)methanol (317.4 mg, 74%). m.p. 107.0–107.3 °C. ^{1}H NMR (400 MHz, $CDCl_3$) δ 7.81 (d, J = 8.1 Hz, 2H, Ph), 7.37–7.31 (m, 4H, Ph), 6.91 (d, J = 8.4 Hz, 2H, Ph), 6.85 (d, J = 8.7 Hz, 2H, Ph), 6.72 (d, J = 8.9 Hz, 2H, Ph), 4.92 (s, 2H, OCH_2), 4.37–4.31 (m, 2H, CH_2), 4.12–4.07 (m, 2H, CH_2), 3.81 (s, 3H, OCH_3), 2.44 (s, 3H, CH_3); ^{13}C NMR (101 MHz, $CDCl_3$) δ 159.46, 153.57, 152.32, 144.89, 133.01, 129.84, 129.18, 128.00, 115.88, 115.76, 114.00, 70.45, 68.27, 66.26, 55.29, 21.62. MS (EI): *m/z* calcd for $C_{23}H_{24}O_6S$ 428; found 428 $[M]^+$.

4.15. 2-(2-(4-((4-methoxybenzyl)oxy)phenoxy)ethoxy)ethyl 4-methylbenzenesulfonate (**4e**)

The reaction described above to prepare **4a** was employed to give **4e** as a colorless oil from **3b** and (4-methoxyphenyl)methanol (298.6 mg, 58%). ^{1}H NMR (400 MHz, $CDCl_3$) δ 7.67 (d, J = 8.3 Hz, 2H, Ph), 7.29 (d, J = 8.2 Hz, 2H, Ph), 7.26 (d, J = 8.6 Hz, 2H, Ph), 6.87 (d, J = 8.7 Hz, 2H, Ph), 6.86 (d, J = 9.2 Hz, 2H, Ph), 6.77 (d, J = 9.1 Hz, 2H, Ph), 4.50 (s, 2H, OCH_2), 4.09–4.05 (m, 2H, CH_2), 3.85–3.81 (m, 2H, CH_2), 3.80 (s, 3H, OCH_3), 3.73–3.70 (m, 2H, CH_2), 3.63–3.60 (m, 2H, CH_2), 2.44 (s, 3H, CH_3); ^{13}C NMR (101 MHz, $CDCl_3$) δ 159.22, 157.47, 145.29, 143.17, 132.24, 130.27, 129.73, 129.38, 128.55, 123.31, 115.20, 113.77, 72.92, 70.90, 69.61, 69.13, 67.84, 55.25, 21.68. MS (ESI): *m/z* calcd for $C_{25}H_{28}NaO_7S$ 495.1; found 495.2 $[M+Na]^+$.

4.16. 2-(2-(2-(4-((4-methoxybenzyl)oxy)phenoxy)ethoxy)ethoxy) ethyl 4-methylbenzenesulfonate (**4f**)

The reaction described above to prepare **4a** was employed to give **4f** as a colorless oil from **3c** and (4-methoxyphenyl)methanol (177.5 mg, 69%). ^{1}H NMR (400 MHz, $CDCl_3$) δ 7.79 (d, J = 7.9 Hz, 2H, Ph), 7.37–7.30 (m, 4H, Ph), 6.93–6.82 (m, 6H, Ph), 4.93 (s, 2H, OCH_2), 4.19–4.13 (m, 2H, CH_2), 4.08–4.02 (m, 2H, CH_2), 3.83–3.76 (m, 5H, CH_2, OCH_3), 3.71–3.58 (m, 6H, CH_2), 2.43 (s, 3H, CH_3); ^{13}C NMR (101 MHz, $CDCl_3$) δ 159.44, 153.25, 153.12, 144.76, 133.17, 129.81, 129.36, 129.18, 127.96, 115.91, 115.66, 113.99, 70.81, 70.75, 70.52, 69.93, 69.25, 68.74, 68.13, 55.29, 21.59. MS (EI): *m/z* calcd for $C_{27}H_{32}O_8S$ 516; found 516 $[M]^+$.

4.17. 4-((4-(2-fluoroethoxy)phenoxy)methyl)-N,N-dimethylaniline (**5a**)

To a solution of **4a** (132.5 mg, 0.30 mmol) in 10 mL of dry THF was added anhydrous TBAF (600 μL, 1 M in THF). The reaction mixture was refluxed for 2 h. Upon completion, the reaction was concentrated and purified by silica gel chromatography (petroleum ether/AcOEt = 3/1, v/v) to give **5a** as a white solid (61.4 mg, 71%). HPLC 13.3 min, 99.2%. m.p. 145.1–145.3 °C. ^{1}H NMR (400 MHz, $CDCl_3$) δ 7.28 (d, J = 8.8 Hz, 2H, Ph), 6.91 (d, J = 9.3 Hz, 2H, Ph), 6.85 (d, J = 9.3 Hz, 2H, Ph), 6.73 (d, J = 8.7 Hz, 2H, Ph), 4.90 (s, 2H, OCH_2), 4.79–4.65 (m, 2H, CH_2), 4.21–4.11 (m, 2H, CH_2), 2.95 (s, 6H, $N(CH_3)_2$); ^{13}C NMR (101 MHz, $CDCl_3$) δ 153.80, 152.64, 150.58, 129.24, 124.77, 115.98, 115.79, 112.56, 82.10 (d, J = 170.4 Hz), 70.90, 67.97 (d, J = 20.5 Hz), 40.61. HRMS (ESI): *m/z* calcd for $C_{17}H_{21}FNO_2$ 290.1551; found 290.1551 $[M+H]^+$.

4.18. 4-((4-(2-(2-fluoroethoxy)ethoxy)phenoxy)methyl)-N,N-dimethylaniline (**5b**)

The reaction described above to prepare **5a** was employed to give **5b** as a white solid from **4b** (56.4 mg, 58%). HPLC 11.5 min, 98.6%. m.p. 111.5–111.8 °C. ^{1}H NMR (400 MHz, $CDCl_3$) δ 7.28 (d, J = 8.6 Hz, 2H, Ph), 6.89 (d, J = 9.2 Hz, 2H, Ph), 6.84 (d, J = 9.2 Hz, 2H, Ph), 6.73 (d, J = 8.6 Hz, 2H, Ph), 4.89 (s, 2H, OCH_2), 4.67–4.50 (m, 2H, CH_2), 4.12–4.07 (m, 2H, CH_2), 3.89–3.75 (m, 4H, CH_2), 2.95 (s, 6H, $N(CH_3)_2$); ^{13}C NMR (101 MHz, $CDCl_3$) δ 153.53, 152.90, 150.53, 129.21, 124.84, 115.90, 115.67, 112.57, 83.18 (d, J = 169.1 Hz), 70.89, 70.58 (d, J = 19.8 Hz), 70.10, 68.22, 40.62. HRMS (ESI): *m/z* calcd for $C_{19}H_{25}FNO_3$ 334.1813; found 334.1812 $[M+H]^+$.

4.19. 4-((4-(2-(2-(2-fluoroethoxy)ethoxy)ethoxy)phenoxy)methyl)-N,N-dimethylaniline (**5c**)

The reaction described above to prepare **5a** was employed to give **5c** as a white solid from **4c** (74.7 mg, 40%). HPLC 9.8 min, 99.1%. m.p. 71.7–72.1 °C. ^{1}H NMR (400 MHz, $CDCl_3$) δ 7.29 (s, 2H, Ph), 6.89 (d, J = 9.2 Hz, 2H, Ph), 6.84 (d, J = 9.2 Hz, 2H, Ph), 6.74 (s, 2H, Ph), 4.90 (s, 2H, OCH_2), 4.64–4.51 (m, 2H, CH_2), 4.11–4.07 (m, 2H, CH_2), 3.87–3.82 (m, 2H, CH_2), 3.81–3.78 (m, 1H, CH_2), 3.76–3.71 (m, 5H, CH_2), 2.97 (s, 6H, $N(CH_3)_2$); ^{13}C NMR (101 MHz, $CDCl_3$) δ 153.41, 152.93, 150.51, 129.22, 124.77, 115.81, 115.58, 112.52, 83.17 (d, J = 169.0 Hz), 70.87, 70.86, 70.83, 70.46 (d, J = 19.7 Hz), 69.95, 68.09, 40.62. HRMS (ESI): *m/z* calcd for $C_{21}H_{29}FNO_4$ 378.2075; found 378.2076 $[M+H]^+$.

4.20. 1-(2-fluoroethoxy)-4-((4-methoxybenzyl)oxy)benzene (**5d**)

The reaction described above to prepare **5a** was employed to give **5d** as a white solid from **4d** (71.7 mg, 87%). HPLC 9.6 min, 96.6%. m.p. 96.8–97.3 °C. ^{1}H NMR (400 MHz, $CDCl_3$) δ 7.34 (d, J = 8.2 Hz, 2H, Ph),

6.94–6.84 (m, 6H, Ph), 4.94 (s, 2H, OCH_2), 4.81–4.64 (m, 2H, CH_2), 4.23–4.11 (m, 2H, CH_2), 3.81 (s, 3H, OCH_3); ^{13}C NMR (101 MHz, $CDCl_3$) δ 159.48, 153.56, 152.80, 129.31, 129.19, 115.99, 115.82, 114.02, 82.05 (d, $J = 170.5$ Hz), 70.52, 67.96 (d, $J = 20.6$ Hz), 55.30. HRMS (EI): *m/z* calcd for $C_{16}H_{17}O_3F$ 276.1162; found 276.1158 $[M]^+$.

4.21. 1-(2-(2-fluoroethoxy)ethoxy)-4-((4-methoxybenzyl)oxy) benzene (**5e**)

The reaction described above to prepare **5a** was employed to give **5e** as a white solid from **4e** (104.8 mg, 63%). HPLC 9.3 min, 98.7%. m.p. 79.9–80.6 °C. ^1H NMR (400 MHz, $CDCl_3$) δ 7.35 (d, $J = 8.6$ Hz, 2H, Ph), 6.93–6.83 (m, 6H, Ph), 4.93 (s, 2H, OCH_2), 4.67–4.52 (m, 2H, CH_2), 4.12–4.07 (m, 2H, CH_2), 3.89–3.84 (m, 3H, CH_2), 3.82 (s, 3H, OCH_3), 3.80–3.77 (m, 1H, CH_2); ^{13}C NMR (101 MHz, CDCl3) δ 159.43, 153.26, 153.04, 129.30, 129.24, 115.85, 115.65, 113.97, 83.18 (d, $J = 169.0$ Hz), 70.57 (d, $J = 19.8$ Hz), 70.45, 70.06, 68.14, 55.29. HRMS (ESI): *m/z* calcd for $C_{18}H_{21}FNaO_4$ 343.1316; found 343.1317 $[M+Na]^+$.

4.22. 1-(2-(2-(2-fluoroethoxy)ethoxy)ethoxy)-4-((4-methoxybenzyl)oxy)benzene (**5f**)

The reaction described above to prepare **5a** was employed to give **5f** as a white solid from **4f** (87.5 mg, 74%). HPLC 9.1 min, 95.4%. m.p. 66.3–66.7 °C. ^1H NMR (400 MHz, $CDCl_3$) δ 7.34 (d, $J = 8.2$ Hz, 2H, Ph), 6.94–6.82 (m, 6H, Ph), 4.93 (s, 2H, OCH_2), 4.56 (d, $J = 47.8$ Hz, 2H, CH_2), 4.09 (s, 2H, CH_2), 3.85–3.70 (m, 11H, CH_2, OCH_3); ^{13}C NMR (101 MHz, $CDCl_3$) δ 159.42, 153.21, 153.13, 129.34, 129.18, 115.87, 115.64, 113.97, 83.13 (d, $J = 169.0$ Hz), 70.85, 70.84, 70.49, 70.44 (d, $J = 19.8$ Hz), 69.93, 68.12, 55.28. HRMS (EI): *m/z* calcd for $C_{20}H_{25}O_5F$ 364.1686; found 364.1680 $[M]^+$.

4.23. 2-(4-formylphenoxy)ethyl 4-methylbenzenesulfonate (**6**)

Compound **6** was prepared through a procedure reported by Divi et al. [26] The reaction described above to prepare **2a** was employed to give **6** as a white solid from 4-(2-hydroxyethoxy) benzaldehyde (3.20 g, 91%). m.p. 101.1–101.7 °C. ^1H NMR (400 MHz, $CDCl_3$) δ 9.89 (s, 1H, CHO), 7.82 (d, $J = 8.4$ Hz, 2H, Ph), 7.81 (d, $J = 8.8$ Hz, 2H, Ph), 7.35 (d, $J = 8.1$ Hz, 2H, Ph), 6.90 (d, $J = 8.7$ Hz, 2H, Ph), 4.43–4.39 (m, 2H, CH_2), 4.26–4.22 (m, 2H, CH_2), 2.45 (s, 3H, CH_3). MS (EI): *m/z* calcd for $C_{16}H_{16}O_5S$ 320; found 320 $[M]^+$.

4.24. 2-(4-(hydroxymethyl)phenoxy)ethyl 4-methylbenzenesulfonate (**7**)

Compound **7** was prepared through a procedure reported by Divi et al. [26] To a stirring mixture of **6** (1.28 g, 4.0 mmol) in anhydrous MeOH (10 mL) in an ice bath, $NaBH_4$ (0.30 g, 8.0 mmol) was slowly added. The reaction mixture was stirred for 30 min at 0 °C and quenched with 10 mL of water. MeOH was evaporated under reduced pressure and the mixture was neutralized with 1 M HCl and then extracted by CH_2Cl_2 (3 × 10 mL). The combined organic layers were dried over anhydrous $MgSO_4$, filtered and concentrated in vacuo to give **7** as a colorless oil (954.6 mg, 74%). ^1H NMR (400 MHz, DMSO-d_6) δ 7.80 (d, $J = 8.3$ Hz, 2H, Ph), 7.48 (d, $J = 8.0$ Hz, 2H, Ph), 7.20 (d, $J = 8.6$ Hz, 2H, Ph), 6.79 (d, $J = 8.6$ Hz, 2H, Ph), 4.40 (s, 2H, CH_2), 4.34–4.30 (m, 2H, CH_2), 4.15–4.11 (m, 2H, CH_2), 2.42 (s, 3H, CH_3). MS (EI): *m/z* calcd for $C_{16}H_{18}O_5S$ 322; found 322 $[M]^+$.

4.25. 2-(4-((4-(dimethylamino)phenoxy)methyl)phenoxy)ethyl 4-methylbenzenesulfonate (**8a**)

The reaction described above to prepare **4a** was employed to give **8a** as a white solid from **7** and 4-(dimethylamino)phenol (56.7 mg, 40%). m.p. 122.5–123.2 °C. ^1H NMR (400 MHz, $CDCl_3$) δ 7.82 (d, $J = 8.3$ Hz, 2H, Ph), 7.34 (d, $J = 8.0$ Hz, 2H, Ph), 7.31 (d, $J = 8.7$ Hz, 2H, Ph), 6.90 (d, $J = 8.9$ Hz, 2H, Ph), 6.83–6.71 (m, 4H, Ph), 4.92 (s, 2H, OCH_2), 4.39–4.34 (m, 2H, CH_2), 4.18–4.12 (m, 2H, CH_2), 2.88 (s, 6H, $N(CH_3)_2$), 2.45 (s, 3H, CH_3); ^{13}C NMR (101 MHz, $CDCl_3$) δ 157.70, 151.25, 145.70, 144.95, 132.87, 130.42, 129.86, 129.13, 127.99, 115.88, 114.85, 114.58, 70.39, 68.11, 65.46, 41.82, 21.64. MS (ESI): *m/z* calcd for $C_{24}H_{28}NO_5S$ 442.2; found 442.2 $[M+Na]^+$.

4.26. 2-(4-((4-methoxyphenoxy)methyl)phenoxy)ethyl 4-methylbenzenesulfonate (**8b**)

The reaction described above to prepare **4a** was employed to give **8b** as a white solid from **7** and 4-methoxyphenol (355.3 mg, 83%). m.p. 100.6–100.9 °C. ^1H NMR (400 MHz, $CDCl_3$) δ 7.82 (d, $J = 8.3$ Hz, 2H, Ph), 7.34 (d, $J = 8.1$ Hz, 2H, Ph), 7.31 (d, $J = 8.6$ Hz, 2H, Ph), 6.89 (d, $J = 9.2$ Hz, 2H, Ph), 6.82 (d, $J = 9.2$ Hz, 2H, Ph), 6.78 (d, $J = 8.6$ Hz, 2H, Ph), 4.92 (s, 2H, OCH_2), 4.39–4.35 (m, 2H, CH_2), 4.17–4.13 (m, 2H, CH_2), 3.77 (s, 3H, OCH_3), 2.45 (s, 3H, CH_3); ^{13}C NMR (101 MHz, $CDCl_3$) δ 157.80, 154.01, 152.94, 144.94, 132.96, 130.21, 129.86, 129.12, 127.99, 115.92 (overlapped), 114.66, 70.39, 68.09, 65.52, 55.72, 21.62. MS (EI): *m/z* calcd for $C_{23}H_{24}O_6S$ 428; found 428 $[M]^+$.

4.27. 4-((4-(2-fluoroethoxy)benzyl)oxy)-N,N-dimethylaniline (**9a**)

The reaction described above to prepare **5a** was employed to give **9a** as a white solid from **8a** (81.7 mg, 88%). HPLC 11.8 min, 99.3%. m.p. 132.9–133.3 °C. ^1H NMR (400 MHz, $CDCl_3$) δ 7.35 (d, $J = 8.0$ Hz, 2H, Ph), 6.96–6.87 (m, 4H, Ph), 6.77 (s, 2H, Ph), 4.94 (s, 2H, OCH_2), 4.75 (d, $J = 47.7$ Hz, 2H, CH_2), 4.22 (d, $J = 27.7$ Hz, 2H, CH_2), 2.88 (s, 6H, $N(CH_3)_2$); ^{13}C NMR (101 MHz, $CDCl_3$) δ 158.18, 151.16, 145.95, 130.37, 129.26, 115.92, 114.74, 114.69, 81.95 (d, $J = 170.6$ Hz), 70.48, 67.19 (d, $J = 20.5$ Hz), 41.74. HRMS (EI): *m/z* calcd for $C_{17}H_{20}NO_2F$ 289.1478; found 289.1481 $[M]^+$.

4.28. 1-(2-fluoroethoxy)-4-((4-methoxyphenoxy)methyl)benzene (**9b**)

The reaction described above to prepare **5a** was employed to give **9b** as a white solid from **8b** (62.9 mg, 91%). HPLC 9.5 min, 98.4%. m.p. 107.5–108.0 °C. ^1H NMR (400 MHz, $CDCl_3$) δ 7.35 (d, $J = 8.5$ Hz, 2H, Ph), 6.97–6.87 (m, 4H, Ph), 6.83 (d, $J = 9.1$ Hz, 2H, Ph), 4.94 (s, 2H, OCH_2), 4.84–4.67 (m, 2H, CH_2), 4.28–4.15 (m, 2H, CH_2), 3.77 (s, 3H, OCH_3); ^{13}C NMR (101 MHz, $CDCl_3$) δ 158.24, 154.01, 152.99, 130.09, 129.20, 115.95, 114.74, 114.67, 81.89 (d, $J = 170.7$ Hz, 1H), 70.45, 67.21 (d, $J = 20.7$ Hz, 1H), 55.71. HRMS (EI): *m/z* calcd for $C_{16}H_{17}O_3F$ 276.1162; found 276.1165 $[M]^+$.

4.29. Radiolabeling

[^{18}F]Fluoride trapped on a Sep-Pak Light QMA (Agela Technologies) cartridge was eluted with 1 mL of Kryptofix222/K_2CO_3 solution (13 mg of Kryptofix222 and 1.1 mg of K_2CO_3 in MeCN/H_2O, 4/1) into a clean glass vial. The solvent was removed and the residue was azeotropically dried with 0.3 mL of anhydrous acetonitrile triple at 120 °C under a stream of nitrogen gas. A solution of the tosylate precursors **4a**, **4d**, **4f**, **8a** or **8b** (5.0 mg) in MeCN (0.5 mL) was added to the reaction vessel containing the $^{18}F^-$ activity and

heated at 100 °C for 5 min. After cooling to room temperature, 10.0 mL of water was added and the mixture was passed through a preconditioned Sep-Pak C18 cartridge (Agela Technologies). The cartridge was washed with 10 mL of water and the labeled compound was then eluted with 1 mL of MeCN. The mixture was concentrated under nitrogen gas and subjected to HPLC purification (Venusil MP C18 column, 5 μm, 10 × 250 mm, CH_3CN/H_2O = 70%/30%, flow rate = 4 mL/min). The preparation took 45 min and the radiochemical yields were approximately 30% (decay corrected). After purification by HPLC, the radiochemical purities were greater than 98% and specific activities were calculated to be approximately 130 GBq/μmol at the end of synthesis.

4.30. Molecular docking and biological evaluation

Molecular docking, biological evaluations including *in vitro* binding assay using Aβ aggregates, *in vitro* autoradiography, partition coefficient determination, *in vivo* biodistribution, *in vivo* metabolism studies and *ex vivo* autoradiography were all conducted according to previously reported methods [11,12].

Acknowledgement

The authors present special thanks to Dr. Jin Liu (College of Life Science, Beijing Normal University) for assistance in the *in vitro* neuropathological staining, and Dr. Xuebing Deng (College of Chemistry, Beijing Normal University) for assistance in the X-ray diffraction. This work was funded by the National Natural Science Foundation of China (No. 21201019) and the National Science and Technology Major Projects for Major New Drugs Innovation and Development (No. 2014ZX09507007-002).

Appendix A. Supplementary data

Supplementary data related to this article can be found at http://dx.doi.org/10.1016/j.ejmech.2015.09.028.

References

[1] J. Hardy, D.J. Selkoe, The amyloid hypothesis of alzheimer's disease: progress and problems on the road to therapeutics,, Science 297 (2002) 353–356.
[2] Y. Yang, M. Cui, Radiolabeled bioactive benzoheterocycles for imaging β-amyloid plaques in Alzheimer's disease, Eur. J. Med. Chem. 87 (2014) 703–721.
[3] M. Cui, Past and recent progress of molecular imaging probes for β-amyloid plaques in the brain, Curr. Med. Chem. 21 (2014) 82–112.
[4] A. Kadir, A. Marutle, D. Gonzalez, M. Schöll, O. Almkvist, M. Mousavi, T. Mustafiz, T. Darreh-Shori, I. Nennesmo, A. Nordberg, Positron emission tomography imaging and clinical progression in relation to molecular pathology in the first Pittsburgh Compound B positron emission tomography patient with Alzheimer's disease, Brain 134 (2011) 301–317.
[5] R. Vandenberghe, K. Van Laere, A. Ivanoiu, E. Salmon, C. Bastin, E. Triau, S. Hasselbalch, I. Law, A. Andersen, A. Korner, L. Minthon, G. Garraux, N. Nelissen, G. Bormans, C. Buckley, R. Owenius, L. Thurfjell, G. Farrar, D.J. Brooks, 18F-flutemetamol amyloid imaging in Alzheimer disease and mild cognitive impairment: a phase 2 trial, Ann. Neurol. 68 (2010) 319–329.
[6] V. Camus, P. Payoux, L. Barré, B. Desgranges, T. Voisin, C. Tauber, R. Joie, M. Tafani, C. Hommet, G. Chételat, K. Mondon, V. Sayette, J.P. Cottier, E. Beaufils, M.J. Ribeiro, V. Gissot, E. Vierron, J. Vercouillie, B. Vellas, F. Eustache, D. Guilloteau, Using PET with 18F-AV-45 (florbetapir) to quantify brain amyloid load in a clinical environment, Eur. J. Nucl. Med. Mol. Imaging 39 (2012) 621–631.
[7] H. Barthel, H.J. Gertz, S. Dresel, O. Peters, P. Bartenstein, K. Buerger, F. Hiemeyer, S. Wittemer-Rmp, J. Seibyl, C. Reininger, O. Sabri, Cerebral amyloid-beta PET with florbetaben (18F) in patients with Alzheimer's disease and healthy controls: a multicentre phase 2 diagnostic study, Lancet Neurol. 10 (2011) 424–435.
[8] C.C. Rowe, V.L. Villemagne, Brain amyloid imaging, J. Nucl. Med. 52 (2011) 1733–1740.
[9] N. Nelissen, K. Van Laere, L. Thurfjell, R. Owenius, M. Vandenbulcke, M. Koole, G. Bormans, D.J. Brooks, R. Vandenberghe, Phase 1 study of the Pittsburgh Compound B derivative 18F-flutemetamol in healthy volunteers and patients with probable Alzheimer disease, J. Nucl. Med. 50 (2009) 1251–1259.
[10] S.M. Landau, B.A. Thomas, L. Thurfjell, M. Schmidt, R. Margolin, M. Mintun, M. Pontecorvo, S.L. Baker, W.J. Jagust, Amyloid PET imaging in Alzheimer's disease: a comparison of three radiotracers, Eur. J. Nucl. Med. Mol. Imaging 41 (2014) 1398–1407.
[11] Y. Yang, M. Cui, X. Zhang, J. Dai, Z. Zhang, C. Lin, Y. Guo, B. Liu, Radioiodinated benzyloxybenzene derivatives: a class of flexible ligands target to β-amyloid plaques in Alzheimer's brains, J. Med. Chem. 57 (2014) 6030–6042.
[12] Y. Yang, X. Zhang, M. Cui, J. Zhang, Z. Guo, Y. Li, X. Zhang, J. Dai, B. Liu, Preliminary characterization and in vivo studies of structurally identical 18F- and 125I-labeled benzyloxybenzenes for PET/SPECT imaging of β-amyloid plaques, Sci. Rep. 5 (2015) 12084.
[13] H. Xi, S. Ju, Z. Chen, X. Sun, Synthesis of N,N'-bis(thioacetoxyalkoxy)piperazine and its aelf-assembled monolayer (SAM) formation on gold electrode, Chem. Lett. 39 (2010) 415–417.
[14] G. Sheldrick, Crystal structure refinement with SHELXL, Acta Crystallogr. C 71 (2015) 3–8.
[15] K.A. Stephenson, R. Chandra, Z.-P. Zhuang, C. Hou, S. Oya, M.-P. Kung, H.F. Kung, Fluoro-pegylated (FPEG) imaging agents targeting Aβ aggregates, Bioconjugate Chem. 18 (2006) 238–246.
[16] M. Cui, X. Wang, P. Yu, J. Zhang, Z. Li, X. Zhang, Y. Yang, M. Ono, H. Jia, H. Saji, B. Liu, Synthesis and evaluation of novel 18F labeled 2-pyridinylbenzoxazole and 2-pyridinylbenzothiazole derivatives as ligands for positron emission tomography (PET) imaging of β-amyloid plaques, J. Med. Chem. 55 (2012) 9283–9296.
[17] W. Zhang, S. Oya, M.-P. Kung, C. Hou, D.L. Maier, H.F. Kung, F-18 polyethyleneglycol stilbenes as PET imaging agents targeting Aβ aggregates in the brain, Nucl. Med. Biol. 32 (2005) 799–809.
[18] F.K. Hank, C. Seok Rye, Q. Wenchao, Z. Wei, S. Daniel, 18F stilbenes and styrylpyridines for PET imaging of A beta plaques in Alzheimer's disease: a miniperspective, J. Med. Chem. 53 (2010) 933–941.
[19] H. Fu, M. Cui, L. Zhao, P. Tu, K. Zhou, J. Dai, B. Liu, High sensitive near-infrared fluorophores for in vivo detection of amyloid-β plaques in Alzheimer's disease, J. Med. Chem. 58 (2015) 6972–6983.
[20] S.R. Choi, G. Golding, Z. Zhuang, W. Zhang, N. Lim, F. Hefti, T.E. Benedum, M.R. Kilbourn, D. Skovronsky, H.F. Kung, Preclinical properties of 18F-AV-45: a PET agent for Aβ plaques in the brain, J. Nucl. Med.50 (2009) 1887–1894.
[21] A.T. Petkova, W.-M. Yau, R. Tycko, Experimental constraints on quaternary structure in Alzheimer's β-amyloid fibrils, Biochemistry 45 (2005) 498–512.
[22] M.J. Frisch, G.W. Trucks, H.B. Schlegel, G.E. Scuseria, M.A. Robb, J.R. Cheeseman, G. Scalmani, V. Barone, B. Mennucci, G.A. Petersson, H. Nakatsuji, M. Caricato, X. Li, H.P. Hratchian, A.F. Izmaylov, J. Bloino, G. Zheng, J.L. Sonnenberg, M. Hada, M. Ehara, K. Toyota, R. Fukuda, J. Hasegawa, M. Ishida, T. Nakajima, Y. Honda, O. Kitao, H. Nakai, T. Vreven, J.A. Montgomery Jr., J.E. Peralta, F. Ogliaro, M. Bearpark, J.J. Heyd, E. Brothers, K.N. Kudin, V.N. Staroverov, T. Keith, R. Kobayashi, J. Normand, K. Raghavachari, A. Rendell, J.C. Burant, S.S. Iyengar, J. Tomasi, M. Cossi, N. Rega, J.M. Millam, M. Klene, J.E. Knox, J.B. Cross, V. Bakken, C. Adamo, J. Jaramillo, R. Gomperts, R.E. Stratmann, O. Yazyev, A.J. Austin, R. Cammi, C. Pomelli, J.W. Ochterski, R.L. Martin, K. Morokuma, V.G. Zakrzewski, G.A. Voth, P. Salvador, J.J. Dannenberg, S. Dapprich, A.D. Daniels, O. Farkas, J.B. Foresman, J.V. Ortiz, J. Cioslowski, D.J. Fox, Gaussian 09, Revision B.01, Gaussian, Inc., Wallingford CT, 2010.
[23] G.M. Morris, D.S. Goodsell, R.S. Halliday, R. Huey, W.E. Hart, R.K. Belew, A.J. Olson, Automated docking using a Lamarckian genetic algorithm and an empirical binding free energy function, J. Comput. Chem. 19 (1998) 1639–1662.
[24] W. Humphrey, A. Dalke, K. Schulten, VMD: Visual molecular dynamics, J. Mol. Graph. Model 14 (1996) 33–38.
[25] J.Z. Hodyl, S. Lincoln, K. Wainwright, Silica-attached molecular receptor complexes for benzoates and naphthoates, J. Incl. Phenom. Macrocycl. Chem. 68 (2010) 261–270.
[26] M.K.P. Divi, G.R. Padakandla, B.N. Rao, D.V. Suresh, Novel process for the preparation of bazedoxifene acetate and intermediates thereof, US 20120330008 A1.